International Journal for Numerical Methods in Fluids

WILEY

RESEARCH ARTICLE OPEN ACCESS

Comparison of Numerical Methods for Geometric Warpage Compensation

Steffen Tillmann[1] | Stefan Basermann[1] | Stefanie Elgeti[1,2]

[1]Chair for Computational Analysis of Technical Systems, RWTH Aachen University, Aachen, Germany | [2]Institute of Lightweight Design and Structural Biomechanics, TU Wien, Vienna, Austria

Correspondence: Steffen Tillmann (tillmann@cats.rwth-aachen.de)

Received: 23 April 2025 | **Revised:** 23 April 2025 | **Accepted:** 21 May 2025

Funding: This work was supported by Deutsche Forschungsgemeinschaft (Grant No. 260064611).

Keywords: algorithm comparison | cavity shape adaptation | injection molding | numerical methods | warpage compensation

ABSTRACT

In injection molding processes, shrinkage and warpage cause deviations in the size and shape of produced parts compared to the cavity shape. While shrinkage is due to the change of material density during solidification, warpage is caused by uneven cooling and internal stresses within the part. One approach to mitigate these effects is by adjusting the cavity shape to anticipate the deformation. While finding the optimal cavity shape is often experience-based in practice, numerical design optimization can greatly assist in this process. In this study, we evaluate various numerical algorithms from existing literature to identify the optimal cavity shape. Each method is briefly outlined regarding how it adapts the geometry, and we discuss their respective strengths and weaknesses for different scenarios. We conduct comparisons using 3D geometries of varying complexity. Our findings demonstrate that, for geometric warpage compensation, the node-based reverse geometry method yields the least warpage and is computationally cost-effective. Furthermore, it is straightforward to implement and consistently performs well across different geometries.

1 | Introduction

Injection molding is one of the most widely used manufacturing processes for plastic products. Naturally, finding new means of increasing both process efficiency and product quality is an ongoing field of research. One key challenge in terms of product quality is the lack of shape accuracy due to shrinkage and warpage. Shrinkage is caused by the density-dependency on both temperature and pressure of plastic melts. Warpage results from uneven shrinkage either due to shape constraints inside the mold or an inhomogeneous temperature distribution within the part during and after solidification [1].

The amount of shrinkage and warpage is influenced by many factors, including material properties, component design, process parameters—such as melt temperature, injection time, injection pressure, holding pressure, and cooling time—and cavity design [2]. Each aspect listed can be optimized to reduce the warpage. For example, materials with a lower thermal expansion coefficient lead to less warpage. The main means of influence with respect to component design is wall thickness. Large, thin-walled parts are particularly prone to warpage [3, 4]. If the wall thickness distribution can be changed from a functional standpoint, warpage can be reduced [5]. For the optimization of process parameters, various algorithms have been utilized, such as genetic algorithms [6, 7], response surface methodology [8–10], Bayesian optimization [11, 12], and particle swarm optimization [2, 13, 14]. Furthermore, there are methods that use locally adjusted cooling to reduce warpage [15, 16].

This article will concentrate on the last category of methods for minimizing warpage, which involves adjusting the mold cavity design to offset the occurring warpage. In this approach, the produced part from the modified cavity shape still undergoes warpage, but it ultimately attains the desired shape after deformation [17]. While this method can be implemented through iterative experiments, repeatedly measuring the newly produced part and adjusting the mold cavity accordingly proves to be both costly and time-consuming [18, 19]. As an alternative, several simulation-based numerical methods have been suggested to calculate the optimal geometry for the cavity shape. We have selected four particularly common methods from the literature. This paper aims to compare these methods in terms of result quality and computational effort. This will enable future users to make an informed choice of the appropriate method for their application. In the following, we will briefly describe the selected methods.

Method 1: The first approach for warpage compensation involves using an inverse model to determine the cavity geometry, as proposed by Zwicke et al. [20–22]. The method begins with a forward simulation to calculate the temperature distribution before part ejection. The inverse model then uses this initial temperature distribution to compute the adjusted cavity shape. This approach is computationally inexpensive, requiring only one forward and one inverse run of the model. However, the initial temperature distribution is computed only once and remains unchanged for the compensated cavity shape. A similar inverse method was used in [23] for 3D printing.

Note that the first method can provide an answer to the optimal cavity shape in one shot. The three remaining methods, on the other hand, are iterative methods.

Method 2: A simple method involves comparing the positions of each mesh node between the deformed and ideal geometries. In each iteration, the cavity geometry is adjusted in the opposite direction of the disparity between the current deformed geometry mesh nodes and the ideal geometry mesh nodes. This method is inspired by experimental cavity shape compensation, where discrete measurements of the produced parts inform adjustments [18, 19, 24]. It should be noted that this so-called reverse geometry method [25] requires identical meshes with corresponding nodes for both the deformed and ideal shapes.

Method 3: Kastelic et al. [25] introduced an alternative method for updating the cavity shape. The method determines the intersection point of the surface normal vector with the ideal geometry and adjusts the surface mesh nodes along the direction of the normal vector to compute the new cavity shape. This method is advantageous when the deformed geometry and the ideal geometry do not share the same mesh. The reverse geometry method and the normal vector method by Kastelic et al. [25] require around five iterations to compute the cavity shape.

Method 4: Another approach involves formulating the problem as a shape optimization task [26]. This can be performed in many different ways, for example, the shape representation can be parametric [27] or nonparametric [28–31]. In this paper, we have selected a spline-based parametrization of the geometry, known as free-form deformation [32]. Here, the position of control points of a spline can deform the geometry, thus serving as the optimization parameters. Subsequently, Bayesian optimization is used as the optimization algorithm [33, 34].

Our paper contributes to the understanding of different warpage compensation methods by providing a comprehensive comparison across several 3D geometries of varying complexity. However, it's important to note that our study does not address the accuracy of predicting the warpage in injection molding. We will begin by presenting the governing equations of our warpage simulation model. Since the primary focus is on the geometry compensation algorithms, we will use a simple warpage model with a linear elastic material model. However, the warpage compensation algorithms can be used with more advanced warpage models if they are available. The following section provides brief explanations of each algorithm, followed by a comprehensive comparison of the methods. Based on the results obtained, we aim to determine the most efficient method for each geometry.

2 | Simulation Model

This section describes the simulation model used in this paper, including the governing equations and boundary conditions. Since the main focus of this article is the assessment of the optimization procedures, the simulation model is kept as simple as possible and comprises two components: A heat conduction simulation and a warpage simulation. The heat conduction simulation is used to determine the initial temperature distribution within the mold cavity prior to part ejection. Subsequently, the warpage simulation calculates the deformation that occurs as the part cools down to ambient temperature after ejection. The simulation model is implemented using the open-source finite element library Nutils [35].

2.1 | Heat Conduction Model

To establish a realistic initial condition for the warpage simulation without conducting a full filling simulation, we solve the heat equation within the cavity domain. The standard heat equation is given by

$$\frac{\partial T}{\partial t} = \kappa \Delta T \text{ in } \Omega \tag{1}$$

where T denotes the temperature and t the time. The computational domain is indicated by Ω, and κ is the thermal diffusivity. The latter is generally dependent on the thermal conductivity, the isobaric heat capacity, and the density, which are itself temperature-dependent. Here, we use a simplified material model with constant κ. As the initial condition, we impose a constant temperature T_I across the part. In addition, we impose a Dirichlet boundary condition T_D on the entire boundary $\partial\Omega$. The boundary temperature T_D is constant over time and is lower than the initial condition. In particular,

$$T_D - T_I = \Delta T_D = -145\text{K on } \partial\Omega \tag{2}$$

The heat conduction simulation is run only for a time period τ, during which the exterior of the part is cooled down while a hot

TABLE 1 | Model parameters.

Parameter	Value
Thermal diffusivity κ	0.13 $mm^2\ s^{-1}$
Heat conduction simulation time τ	10 s
Ambient temperature T_a	15°C
Material name	Pocan B1305 000000
Thermal expansion coefficient α	$1.1 \cdot 10^{-4}\ K^{-1}$
First Lamé constant λ	4 GPa
Second Lamé constant μ	1 GPa

core remains. The resulting temperature field is called T_0 and is used in the subsequent warpage simulation. The utilized parameters of the heat equation simulation are given in Table 1, which also contains the parameters of the following warpage model.

2.2 | Warpage Model

The warpage simulation approximates the deformation of the material due to shrinkage and warpage after ejection. The polybutylene terephthalate (PBT) used as the material in the simulation is Pocan B1305 000000 from Envalior GmbH. We assume a fully solidified, isotropic, and stress-free material with linear elasticity as a simplification. The problem is described by the linear thermoelastic constitutive equation, also known as the Duhamel-Neumann law [36], which is given by:

$$\boldsymbol{\sigma} = \lambda\ \mathrm{tr}(\boldsymbol{\varepsilon})\mathbf{1} + 2\mu\boldsymbol{\varepsilon} - \alpha(3\lambda + 2\mu)(T_a - T_0)\mathbf{1} \tag{3}$$

Here, $\boldsymbol{\sigma}$ denotes the stress, $\boldsymbol{\varepsilon}$ the strain, and α the thermal expansion coefficient. The temperatures T_a and T_0 represent the ambient and initial temperature respectively, λ and μ are the first and second Lamé constants. In our case, the ambient temperature T_a is uniform, and the initial temperature T_0 is nonuniform as described in Section 2.1. This nonuniform temperature change induces thermal stresses, as different parts of the geometry experience various levels of thermal expansion. The thermal stresses induce mechanical strains with a linear elastic relation. For further reading, refer to [37, 38]. The utilized values are summarized in Table 1.

3 | Arrangement for Method Comparison

This section provides a detailed description of the setup utilized for comparing the methods. We commence by presenting a summary of each method under consideration. Additionally, we elaborate on the test geometries and the quality criteria employed to assess the methods.

3.1 | Numerical Methods

3.1.1 | Inverse Shape Design

In [21], the authors introduce the inverse shape design method, which aims to calculate the optimal shape of the cavity directly. The concept entails creating an inverse warpage simulation. The desired shape is used as input, and the unknown cavity shape is the output. Under certain assumptions, it is indeed possible to create an inverse model. The requirements for this task are to restrict the simulation to warpage and allow enough time for cool-down to reach a steady-state solution. Note that linear material behavior is explicitly not a requirement. Additionally, an approximation of the initial temperature field is required as the final cavity shape is unknown prior to the simulation. To estimate the temperature field in the final cavity shape, we use the temperature field computed for a cavity that matches the desired geometry. For a more accurate temperature approximation, please refer to [39]. Note that this is an intrusive method that requires access to the source code of the simulation model for implementation. So either open source software is required, or the companies developing the commercial simulation tools must implement the inverse method themselves.

3.1.2 | Reverse Geometry Method

The reverse geometry method is an iterative technique that corrects the cavity shape by adjusting the mesh coordinates in the opposite direction of the deviation from the desired shape. That is, starting from an initial estimate of the cavity, a forward warpage simulation is performed. The deviation between the warped geometry and the ideal geometry is the basis for the cavity shape correction. Consider the following: $\mathbf{x}_i$ represents the mesh coordinates of the cavity shape in iteration i. The deformed domain resulting from the warpage simulation is denoted by $\tilde{\mathbf{x}}_i$, and the ideal shape is denoted by $\mathbf{x}_{\text{ideal}}$. The update scheme is then given by:

$$\mathbf{x}_0 = \mathbf{x}_{\text{ideal}} \tag{4}$$

for the first iteration, and the following iterations by:

$$\mathbf{x}_{i+1} = \mathbf{x}_{\text{ideal}} - (\tilde{\mathbf{x}}_i - \mathbf{x}_i) \tag{5}$$

The advantages of the method are that the computational cost does not scale with the complexity of the geometry, and the implementation is simple. The disadvantage is that the method does not work directly if the geometry is re-meshed, meaning that the same mesh is not available for both the ideal and the deformed geometry.

3.1.3 | Normal Vector Method

The normal vector method, developed by Kastelic et al. [25], involves an iterative adjustment of the cavity shape. This adjustment is carried out by computing the normal vector at each surface node of the warped geometry mesh and identifying its intersection point with the corresponding desired geometry surface. Subsequently, the mesh coordinates of the cavity shape are modified based on the displacement vector between the warped mesh node and the intersection point.

It is important to note that there is no guarantee that the normal vector at a mesh node of the deformed geometry will intersect the desired geometry surface. To address this, surfaces may

need to be extended to ensure the identification of an intersection point. In addition, since moving mesh nodes only in the direction of the surface normal can result in an irregular mesh, mesh regularization techniques must be incorporated. The method offers advantages such as localized computation of changes and non-intrusiveness. However, it has the disadvantage of requiring additional computations, and mesh regularization requires an appropriate choice of hyperparameters to be set for each geometry. The hyperparameters include an angle for edge detection of the surface splitting, which should be around 90 deg or smaller, depending on whether the geometry has smaller degree angles at corners. If it is too small, edges can be detected falsely. The next hyperparameter is how much the split surfaces are extended. This depends on how much warpage occurs; in our case, extending the surfaces by a factor of three worked fine. Another important hyperparameter is the radius for the radial basis function-based elastic mesh update regularization. This should be in the order of magnitude of around ten times the mesh size.

Remark. The normal vector method, when applied exactly as described in [25], faces challenges when it comes to geometries with intricate details such as small holes or ribs. To overcome this problem, additional steps are required to accurately locate the intersection points of the associated normal vectors.

3.1.4 | Shape Optimization With Bayesian Optimization

Bayesian optimization (BO) is a powerful technique used in robust optimization to find optimal solutions for complex problems with uncertainty or variability in the system. BO combines probabilistic modeling with optimization to efficiently find the best solution in a noisy or uncertain environment. It uses an acquisition function, such as expected improvement or probability of improvement, to balance exploration (sampling uncertain regions) and exploitation (sampling promising regions) of the parameter space. The acquisition function guides the search for the best solution while considering uncertainty. In the frame of robust optimization, BO is strongly interlinked with Gaussian process regression. Refer to [33, 34, 40] for further reading.

How BO can be used in cavity design is described in detail in [26]. Here, we give a brief recap. When approaching the warpage compensation problem as a shape optimization problem, the first ingredient that needs to be determined is the objective function J. Here, we use a mesh-based measure that sums the squared distance between the ideal and deformed shapes at each mesh node. This yields:

$$J = \sqrt{\frac{1}{N}\sum_{j=0}^{N} ||\mathbf{x_{ideal,j}} - \tilde{\mathbf{x}}_\mathbf{j}||_2^2} \tag{6}$$

where $\mathbf{x_{ideal}}$ and $\tilde{\mathbf{x}}$ are the mesh node coordinates of the ideal and deformed shape. Additionally, N is the total number of mesh nodes, and j indicates the number of the mesh node. So, for each mesh node, the distance between the ideal shape and the warped shape is computed and averaged over the whole part by computing the root mean square value. For the deformation and parametrization of the geometry, the free-form deformation method [32] is employed. In this method, the finite element mesh is embedded in a box-spline. The positions of the spline control points then serve as optimization parameters. Our study uses a quadratic B-spline with three evenly distributed control points in each coordinate direction. As these control point positions are adjusted, the mesh also deforms. Bayesian optimization begins by running the forward simulation model with a small initial set of random inputs. Using this data, the Gaussian process regression surrogate model is trained. The optimal next values for balancing exploration and exploitation lie at the global minimum of the acquisition function. An optimizer seeks the global optimum of the acquisition function, which is then chosen as the next training point.

As the BO method is a shape optimization-based approach, it can incorporate additional optimization goals or constraints. For example, the injection molding process parameters, like the cooling rate or the plastic melt temperature, can be added as optimization parameters. Also, geometric constraints regarding the parts' demoldability can be added, as well as constraints to avoid manufacturing defects, such as sink marks or flow lines. However, this comes with the downside of higher computational cost.

3.2 | Evaluation Metric

To compare the effectiveness of the different methods, we need an evaluation measure of the current warpage. For the reverse geometry method, the Bayesian optimization approach, and the inverse method, we use Equation (6). This is the objective function used in the Bayesian optimization approach, which calculates the mesh node-based root mean square (RMS) difference. Since the normal vector method moves the mesh nodes parallel to the surface for regularization purposes, we cannot use the node-to-node difference. Instead, we compute the objective function with the squared average of the distance $\mathbf{d}$ between the mesh nodes of the deformed surface and the ideal surface:

$$J = \sqrt{\frac{1}{N}\sum_{j=0}^{N} ||\mathbf{d_j}||_2^2} \tag{7}$$

In the results section, these metrics are normalized to the initial value of one or 100%, meaning there is the initial amount of warpage without compensation. For each geometry, the normalization (8) is done with the initial warpage of the undeformed geometry. Depending on the method, J is computed with (6) or (7). This allows for a meaningful comparison between the different geometries.

$$J_{\text{normalized}} = \frac{J}{J_{\text{initial}}} \tag{8}$$

3.3 | Test Geometries

To perform the comparison, a wide range of geometries is used. Figure 1 gives an overview of these five 3D geometries with different levels of complexity. The edge lengths for these parts range from 30 to 300 mm. Geometry A (Figure 1a) is a box with a semi-cylindrical opening, and geometry B (Figure 1b) is a parallelogram-shaped part. Geometry C (Figure 1c) is a symmetrical part with boxes and fins, geometry D (Figure 1d) is a box

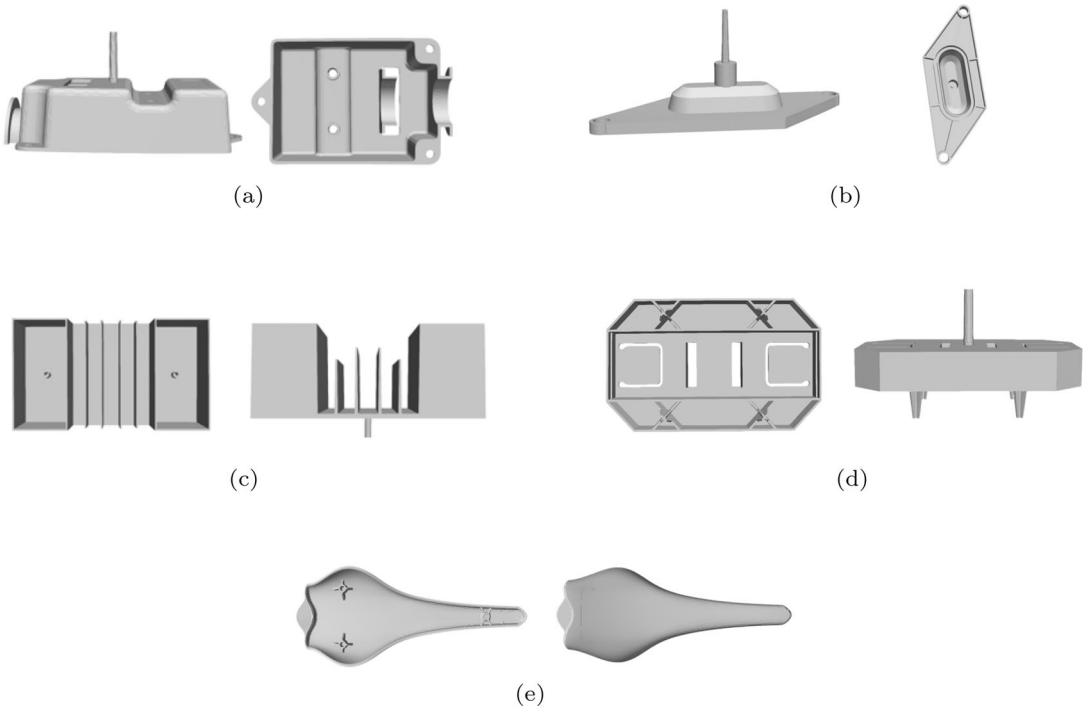

FIGURE 1 | The five geometries A – E, which are used as test cases for the methods. (a) Box-shaped geometry A with a half cylindrical opening, (b) Geometry B with a parallelogram-shaped base, (c) Geometry C with fins and two upwards opened boxes, (d) Geometry D with cross-shaped installation mounts and U-shaped holes, and (e) Bicycle saddle geometry E.

with cross-shaped fins, and geometry E (Figure 1e) is a bicycle saddle.

4 | Numerical Results

This section presents the outcomes of the comparison among the various methods. Initially, the results obtained from the Bayesian optimization method, the inverse method, the reverse geometry method, and the normal vector method are presented for the five geometries. Subsequently, we compare the results of the methods.

4.1 | Results of the Shape Optimization With Bayesian Optimization Method

In this section, the results of the shape optimization approach are presented and discussed. The convergence of the RMS measure (Equation 6) over 300 iterations for each of the five geometries is displayed in Figure 2. The Bayesian optimization algorithm decreased the warpage in the best case of geometry E (Figure 1e) to 45% and in the worst case of geometry D (Figure 1d) to only 80% of the initial warpage. It should be noted that throughout the iterations of each geometry, there are sections where the RMS does not decrease. This happens when the computed training point of the Bayesian optimization algorithm is utilized for exploring the domain.

4.2 | Results of the Inverse Method

In Table 2, the results of the inverse method are shown for each geometry. For every geometry, the warpage is reduced to roughly 1% of its initial value. The inverse method worked best on geometry D (Figure 1d) with a reduction to 1.05% and worst on geometry C (Figure 1c) with 1.52%. This shows that the inverse method is an effective tool to reduce the warpage regardless of the complexity of the geometry. Additionally, the inverse method is computationally much cheaper than the Bayesian optimization method, as it only requires one iteration instead of 300 iterations.

4.3 | Results of the Reverse Geometry Method

Now we are showing the results of the reverse geometry method applied to all geometries (Figure 3). Note that the y-axis of the figure is a logarithmic scale and only five iterations are shown. The warpage is reduced to between around $10^{-4}\%$ and below $10^{-7}\%$ of its initial value depending on the geometry. This method requires significantly fewer iterations than the Bayesian optimization method and results in a greater reduction in warpage. As mentioned before, in the case of a linear elastic material law, the first iteration of the reverse geometry method and the inverse method lead to the same result. However, the reverse geometry method further reduces the warpage in subsequent iterations.

4.4 | Results of the Normal Vector Method

The results of the normal vector method for the given five geometries are visualized in Figure 4. For all geometries, the warpage exhibits the greatest decrease during the initial three iterations, after which the rate of decrease gradually slows. For geometries B (Figure 1b), C (Figure 1c), and E (Figure 1e), the RMS difference was reduced to below 1% of its initial value in five iterations.

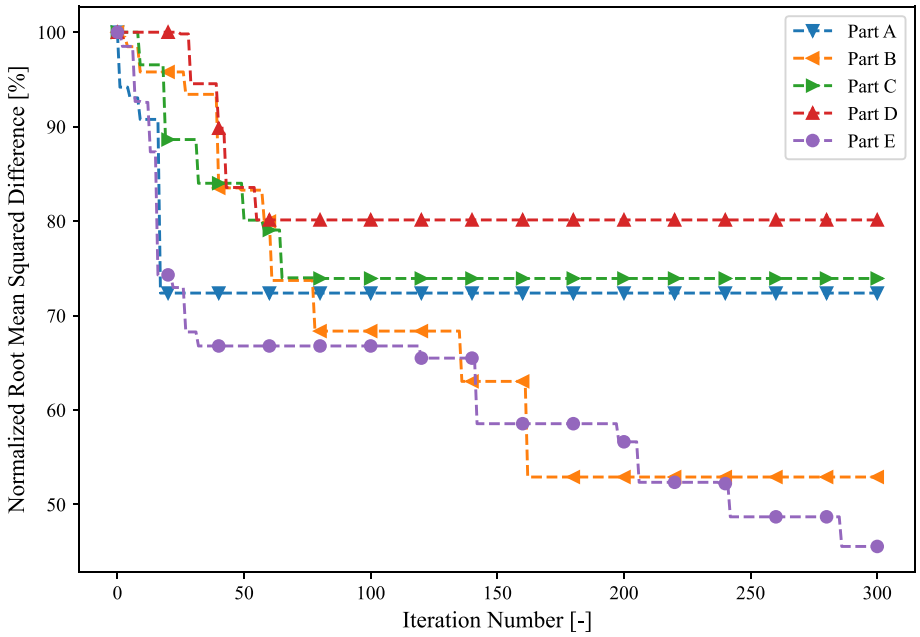

FIGURE 2 | Convergence of the normalized RMS difference on a logarithmic scale for the geometries A–E with the shape optimization method. The RMS difference measures the difference between the warped part and the ideal geometry. The x-axis shows the number of iterations. [Colour figure can be viewed at wileyonlinelibrary.com]

TABLE 2 | Remaining warpage after using the inverse method. Shown is the normalized RMS difference in percent between the initial shape and the resulting shape.

Geometry	Remaining warpage from initial shape
A	1.14%
B	1.05%
C	1.52%
D	1.17%
E	1.38%

The method demonstrated the least effectiveness for geometry D (Figure 1d), with a reduction in warpage below 2.5% of its starting value. In summary, the method demonstrated a notable reduction in warpage for all five geometries. It should be noted, however, that for each geometry, a separate hyperparameter tuning was necessary. The lack of further reduction in warpage below 1% could be attributed to the inability of the normal vector method to compensate for fine features accurately.

4.5 | Comparison of the Methods

The present study compares the warpage reduction of the four different methods. Table 3 presents the remaining warpage for each of the five geometries. In general, the reverse geometry demonstrated the most effective reduction in the objective function. The normal vector method is the second-best performer, followed by the inverse method. The Bayesian optimization method demonstrated the least efficacy in reducing warpage, despite running for 300 iterations, in comparison to the five iterations of the reverse and normal vector methods. The inverse method is the least computationally expensive method, requiring only one iteration. However, its warpage reduction is inferior to that of the reverse geometry method, which requires five iterations. Additionally, the inverse method is not suitable for industrial applications due to its incompatibility with commercial simulation software. The normal vector method showed a significant reduction in warpage, although less than the reverse geometry method. Furthermore, the normal vector method is more computationally expensive than the reverse geometry method, as it necessitates the calculation of normals, surface extensions, and mesh smoothing operations, which are additional overheads. Furthermore, the normal vector method necessitates the tuning of specific hyperparameters, a process that the reverse geometry method does not require.

5 | Discussion and Outlook

While we use a simplified material model, it is enough to compare the methods accurately. This is supported by the fact that we have used the reverse geometry method with a more advanced material model with the commercial simulation software Moldflow, and the first results showed similar performance to that of the simplified material model [41].

The numerical findings indicate that the Bayesian optimization method requires a significantly higher number of iterations compared to the other methods. In fact, the method is simply too powerful for the performed design test, and its practical utility is only evident when the geometric compensation of the cavity shape is integrated with additional optimization objectives. For example, the injection molding process parameters could be optimized simultaneously, or geometric constraints could be added, which the other methods cannot. Instead, the inverse method yields promising results, but being an intrusive approach, it is difficult to use in industrial applications using commercial

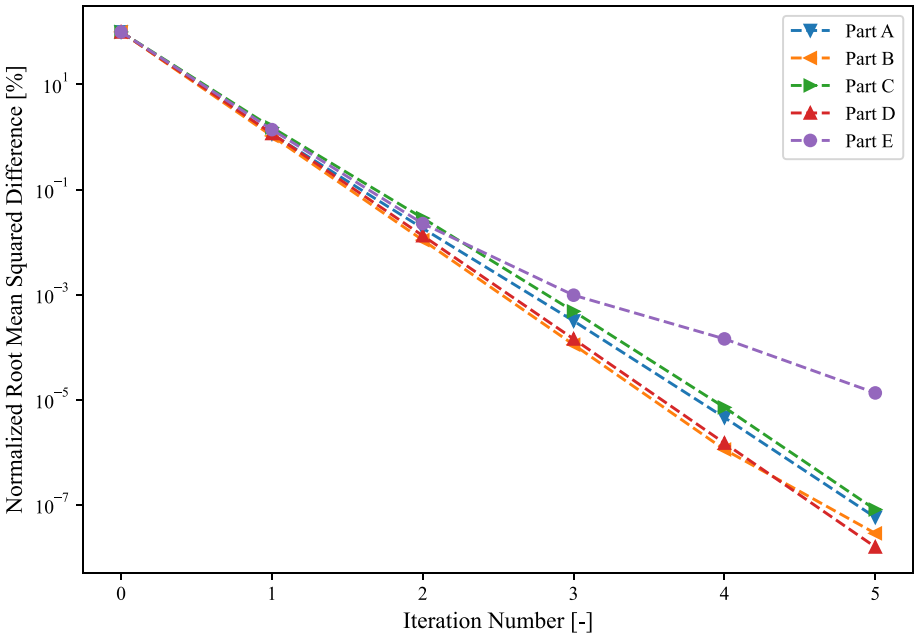

FIGURE 3 | Convergence of the normalized RMS difference for the geometries A–E with the reverse geometry method. The RMS difference measures the difference between the warped part and the ideal geometry. The x-axis shows the number of iterations. [Colour figure can be viewed at wileyonlinelibrary.com]

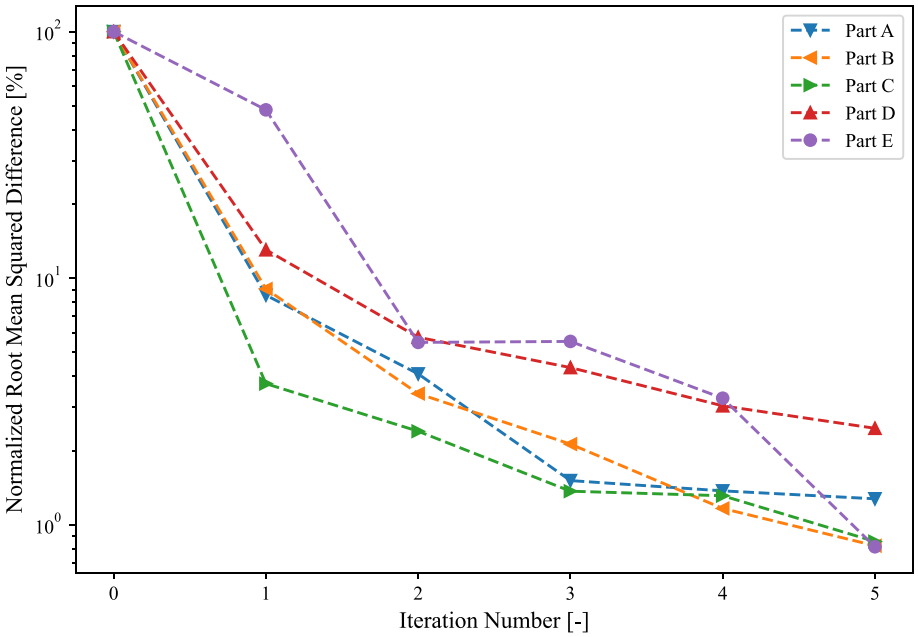

FIGURE 4 | Convergence of the normalized RMS difference for the geometries A–E with the normal vector method. The RMS difference measures the difference between the warped part and the ideal geometry. The x-axis shows the number of iterations. [Colour figure can be viewed at wileyonlinelibrary.com]

simulation tools. To implement the inverse method, access to the source code is required, and thus, it needs to be implemented by the companies developing the commercial simulation tools. Otherwise, open-source simulation software needs to be used.

Overall, the normal vector method and the reverse geometry method yielded the most favorable results, with the reverse geometry method demonstrating superior performance in the tested geometry. While the practical significance of this better performance may be debated, it's crucial to acknowledge that the normal vector method encounters difficulties in accommodating small geometric features. Furthermore, achieving satisfactory results in shape regularization with the normal vector method requires hyperparameter tuning.

The reverse geometry works on any geometry without additional effort or hyperparameter tuning, and it is straightforward to implement. It has to be noted that the reverse geometry

TABLE 3 | Comparison of the four investigated warpage compensation methods. For each geometry and method, the remaining warpage measured by the normalized RMS difference in percent is shown.

Geometry	Shape optimization	Reverse geometry	Normal vector	Inverse
A	72.38%	$5.82 \cdot 10^{-8}$%	1.27%	1.14%
B	52.91%	$2.88 \cdot 10^{-8}$%	0.82%	1.05%
C	73.93%	$8.17 \cdot 10^{-8}$%	0.86%	1.52%
D	80.13%	$1.59 \cdot 10^{-8}$%	2.46%	1.17%
E	45.56%	$1.35 \cdot 10^{-5}$%	0.82%	1.38%

method does not work directly when the desired geometry and the deformed geometry are not available in the same mesh. This can happen when the simulation model forces a remeshing of the geometry in the subsequent iterations of the reverse geometry method. Further research will be done to overcome this problem by applying interpolation methods to the remeshed geometry.

Acknowledgments

The presented investigations were carried out at RWTH Aachen University within the framework of the Collaborative Research Centre SFB1120-236616214 "Bauteilpräzision durch Beherrschung von Schmelze und Erstarrung in Produktionsprozessen" and funded by the Deutsche Forschungsgemeinschaft e.V. (DFG, German Research Foundation). The sponsorship and support are gratefully acknowledged.

Computations were performed with computing resources granted by RWTH Aachen University under project thes1520. Open Access funding enabled and organized by Projekt DEAL.

Data Availability Statement

The data and materials for this publication are available on request at the following link http://hdl.handle.net/21.11102/fba44999-641c-46f6-b076-034f1d0a3303.

References

1. J. M. Fischer, "2 - Shrinkage and Warpage," in *Handbook of Molded Part Shrinkage and Warpage*, 2nd ed., ed. J. M. Fischer (Plastics Design Library, William Andrew Publishing, 2013), 9–17, https://doi.org/10.1016/B978-1-4557-2597-7.00002-1.

2. N.-y. Zhao, J.-y. Lian, P.-f. Wang, and Z.-b. Xu, "Recent Progress in Minimizing the Warpage and Shrinkage Deformations by the Optimization of Process Parameters in Plastic Injection Molding: A Review," *International Journal of Advanced Manufacturing Technology* 120, no. 1–2 (2022): 85–101.

3. R. Azad and H. Shahrajabian, "Experimental Study of Warpage and Shrinkage in Injection Molding of Hdpe/Rpet/Wood Composites With Multiobjective Optimization," *Materials and Manufacturing Processes* 34, no. 3 (2019): 274–282.

4. Y. Chen and J. Zhu, "Warpage Analysis and Optimization of Thin-Walled Injection Molding Parts Based on Numerical Simulation and Orthogonal Experiment," *IOP Conference Series: Materials Science and Engineering* 688 (2019): 33027.

5. B. Lee and B. Kim, "Variation of Part Wall Thicknesses to Reduce Warpage of Injection-Molded Part: Robust Design Against Process Variability," *Polymer-Plastics Technology and Engineering* 36, no. 5 (1997): 791–807.

6. J. Zhao, G. Cheng, S. Ruan, and Z. Li, "Multi-Objective Optimization Design of Injection Molding Process Parameters Based on the Improved Efficient Global Optimization Algorithm and Non-Dominated Sorting-Based Genetic Algorithm," *International Journal of Advanced Manufacturing Technology* 78 (2015): 1813–1826.

7. K. Li, S. Yan, Y. Zhong, W. Pan, and G. Zhao, "Multi-Objective Optimization of the Fiber-Reinforced Composite Injection Molding Process Using Taguchi Method, Rsm, and Nsga-Ii," *Simulation Modelling Practice and Theory* 91 (2019): 69–82.

8. B. S. Heidari, E. Oliaei, H. Shayesteh, et al., "Simulation of Mechanical Behavior and Optimization of Simulated Injection Molding Process for Pla Based Antibacterial Composite and Nanocomposite Bone Screws Using Central Composite Design," *Journal of the Mechanical Behavior of Biomedical Materials* 65 (2017): 160–176.

9. M. Rosli, S. A. Termizi, C. Khor, M. Nawi, A. A. Omar, and M. I. Ishak, "Simulation Based Optimization of Thin Wall Injection Molding Parameter Using Response Surface Methodology," *IOP Conference Series: Materials Science and Engineering* 864 (2020): 012193.

10. S. Rizvi, A. K. Singh, and G. R. Bhadu, "Optimization of Tensile Properties of Injection Molded αi-Nucleated Polypropylene Using Response Surface Methodology," *Polymer Testing* 60 (2017): 198–210.

11. X. Wang, J. Gu, C. Shen, and X. Wang, "Warpage Optimization With Dynamic Injection Molding Technology and Sequential Optimization Method," *International Journal of Advanced Manufacturing Technology* 78 (2015): 177–187.

12. H. Li, K. Liu, D. Zhao, M. Wang, Q. Li, and J. Hou, "Multi-Objective Optimizations for Microinjection Molding Process Parameters of Biodegradable Polymer Stent," *Materials* 11, no. 11 (2018): 2322.

13. Y. Xu, Q. Zhang, W. Zhang, and P. Zhang, "Optimization of Injection Molding Process Parameters to Improve the Mechanical Performance of Polymer Product Against Impact," *International Journal of Advanced Manufacturing Technology* 76 (2015): 2199–2208.

14. J. Zhang, J. Wang, J. Lin, Q. Guo, K. Chen, and L. Ma, "Multiobjective Optimization of Injection Molding Process Parameters Based on Opt Lhd, Ebfnn, and Mopso," *International Journal of Advanced Manufacturing Technology* 85 (2016): 2857–2872.

15. S. Kitayama, Y. Yamazaki, M. Takano, and S. Aiba, "Numerical and Experimental Investigation of Process Parameters Optimization in Plastic Injection Molding Using Multi-Criteria Decision Making," *Simulation Modelling Practice and Theory* 85 (2018): 95–105.

16. C. Hopmann and P. Nikoleizig, "Inverse Thermal Mold Design for Injection Molds: Adressing the Local Cooling Demand as Quality Function for an Inverse Heat Transfer Problem," *International Journal of Material Forming* 11 (2018): 113–124.

17. M. Keuerleber and P. Eyerer, "Gestalten, Fügen, Berechnungsansätze und Simulation EDV-Unterstützter Konstruktionen und Auslegung von Kunststoffbauteilen," in *Polymer Engineering: Technologien und Praxis*, 1st ed. (Springer, 2008), 466–485, https://doi.org/10.1007/978-3-540-72419-3.

18. R. Schlutter, *Einstieg in die Spritzgießsimulation* (Carl Hanser Verlag GmbH Co KG, 2023).

19. H. Zhai, Y. Chang, X. Li, et al., "A research method to improve the quality of box-type thin-walled parts by combining parameter optimization and inverse-deformation design," 2022.

20. F. Zwicke, M. Behr, and S. Elgeti, "Predicting Shrinkage and Warpage in Injection Molding: Towards Automatized Mold Design," in *AIP Conference Proceedings*, vol. 1896 (AIP Publishing, 2017).

21. F. Zwicke and S. Elgeti, "Inverse Design Based on Nonlinear Thermoelastic Material Models Applied to Injection Molding," *Finite Elements in Analysis and Design* 165 (2019): 65–76.

22. F. Zwicke, T. Hohlweck, C. Hopmann, and S. Elgeti, "Inverse Design Based on Nonlinear Thermoelastic Material Models," *PAMM* 20, no. 1 (2021): 202000130.

23. T. Hanuhov and N. Cohen, "Design Principles for 3d-Printed Thermally Activated Shape-Morphing Structures," *International Journal of Mechanical Sciences* 262 (2024): 108716.

24. H. Zhai, X. Li, X. Xiong, et al., "A Method Combining Optimization Algorithm and Inverse-Deformation Design for Improving the Injection Quality of Box-Shaped Parts," *International Journal of Advanced Manufacturing Technology* 130 (2023): 1901–1924.

25. T. Kastelic, B. Starman, G. Cafuta, M. Halilovic, and N. Mole, "Correction of Mould Cavity Geometry for Warpage Compensation," *International Journal of Advanced Manufacturing Technology* 123, no. 5–6 (2022): 1957–1971.

26. S. Tillmann, M. Behr, and S. Elgeti, "Using Bayesian Optimization for Warpage Compensation in Injection Molding," *Materialwissenschaft und Werkstofftechnik* 55, no. 1 (2024): 13–20, https://doi.org/10.1002/mawe.202300157.

27. H. Azegami, *Shape Optimization Problems* (Springer, 2020).

28. M. Hojjat, E. Stavropoulou, and K.-U. Bletzinger, "The Vertex Morphing Method for Node-Based Shape Optimization," *Computer Methods in Applied Mechanics and Engineering* 268 (2014): 494–513.

29. K. C. Giannakoglou and D. I. Papadimitriou, "Adjoint Methods for Shape Optimization," in *Optimization and Computational Fluid Dynamics* (Springer Berlin Heidelberg, 2008), 79–108.

30. A. Jameson, "Aerodynamic shape optimization using the adjoint method. Lectures at the Von Karman Institute, Brussels," 2003.

31. C. Le, T. Bruns, and D. Tortorelli, "A Gradient-Based, Parameter-Free Approach to Shape Optimization," *Computer Methods in Applied Mechanics and Engineering* 200, no. 9–12 (2011): 985–996.

32. T. W. Sederberg and S. R. Parry, "Free-Form Deformation of Solid Geometric Models," in *Proceedings of the 13th Annual Conference on Computer Graphics and Interactive Techniques* (Association for Computing Machinery, 1986), 151–160.

33. B. Shahriari, K. Swersky, Z. Wang, R. P. Adams, and N. De Freitas, "Taking the Human out of the Loop: A Review of Bayesian Optimization," *Proceedings of the IEEE* 104, no. 1 (2015): 148–175.

34. P. I. Frazier, "A Tutorial on Bayesian Optimization," 2018, arXiv preprint arXiv:1807.02811.

35. J. S. B. Zwieten, G. J. Zwieten, and W. Hoitinga, "Nutils 7.0. Zenodo," 2022, https://doi.org/10.5281/zenodo.6006701.

36. M. H. Sadd, *Elasticity: Theory, Applications, and Numerics* (Academic Press, 2009).

37. M. P. Nemeth, "An In-Depth Tutorial on Constitutive Equations for Elastic Anisotropic Materials. Technical Report," 2011.

38. H. Parkus, *Thermoelasticity* (Springer, 2012).

39. F. Zwicke, M. Behr, and K. Veroy, "Inverse Shape Design in Injection Molding Based on the Finite Element Method. (PhD thesis)," 2020.

40. R. Garnett, *Bayesian Optimization* (Cambridge University Press, 2023).

41. S. Tillmann, S. Schwan, D. C. Fritsche, C. E. Kahve, S. Elgeti, and C. Hopmann, "Using the Reverse Geometry Method for Warpage Compensation on Changing Meshes With Interpolation Methods," *PAMM* 24, no. 4 (2024): 202400010.